PCCP

Accepted Manuscript

ROYAL SOCIETY OF CHEMISTRY

rsc.li/pccp

View Article Online
DOI: 10.1039/C8CP06912C

PCCP

ARTICLE TYPE

Cite this: DOI: 10.1039/xxxxxxxxxx

In-situ XPS analysis of the atomic layer deposition of aluminium oxide on titanium dioxide†

Robert H. Temperton,[a‡] Andrew Gibson[a], James N. O'Shea*[a]

Received Date
Accepted Date

DOI: 10.1039/xxxxxxxxxx

www.rsc.org/journalname

Ultra-thin aluminium oxide was grown on a rutile titanium dioxide surface by atomic layer deposition using trimethylaluminium and water precursors. This process, carried out using realistic temperatures and pressures (1 mbar, 450 K), was monitored in-situ using near-ambient pressure X-ray photoelectron spectroscopy (NAP-XPS). This provides insight into the surface chemistry at the interface between the two oxide layers - specifically the reduction of titanium atoms from Ti^{4+} to Ti^{3+} upon dosing of trimethylaluminium. These defect states become locked into the heterojunction's interface, with implications to its electronic structure, and can act as an indicator as to when complete coverage of the rutile substrate is achieved.

1 Introduction

The ability to grow ultra-thin aluminium oxide layers on titanium dioxide is of interest to molecular devices such as dye sensitised solar cells[1]. These commonly consist of a TiO_2 electrode with a monolayer of dye chemically anchored to it, a redox electrolyte and a catalytic counter electrode. A challenge in optimising the performance of these devices is controlling the recombination of electrons from the TiO_2 electrode into either the dye or the electrolyte[2]. The introduction of an ultra-thin alumina layer, placed between the underlying titania and the absorbed dye molecules, has been shown to achieve this. The reported improvements in power conversion efficiency are attributed to the alumina passivating the underlying titania surface and providing an energy barrier blocking recombination processes by shifting the conduction band of the surface to higher energies[3–6]. Furthermore, using aluminium oxide has also been shown to increase dye adsorption[7].

Our previous work has included photoemission studies of the "N3" dye* absorbed on an ultra-thin aluminium oxide layer (grown on a nickle aluminium single crystal)[8]. However, growing such a film on titanium dioixde is a more challenging problem where getting repeatable ultra-thin films (a few monolayers) without contaminants at the interface is required. By exposing the surface to an alternating series of reactants, atomic layer deposition (ALD) can achieve just this[9,10]. ALD of aluminium oxide using trimethylaluminum (TMA), $Al(CH_3)_3$, and water is considered a model ALD process since the reactants are highly reactive, thermally stable and the reaction by-product, methane, does not interfere with the growth process[11,12]. The growth of aluminium oxide by ALD is described by the following two half equations[13]:

$$M\text{-}OH + Al(CH_3)_3 \longrightarrow M\text{-}O\text{-}Al(CH_3)_2 + CH_4 \quad (1)$$

$$M\text{-}O\text{-}Al(CH_3)_2 + 2\,H_2O \longrightarrow M\text{-}O\text{-}Al\text{-}(OH)_2 + 2\,CH_4 \quad (2)$$

Here, M-O describes the surface metal-oxide (whether Ti-O initially or Al-O for subsequent layers). In reaction 1, we see a methyl ((CH3)) group dissociating from the TMA molecule on reaction with surface oxygen atoms. In reaction 2, we see water stripping away the further two methyls. Repeating these two "half-cycles" allows us to build up films of aluminium oxide to whatever thickness is required. It is also worth noting that each cycle is unlikely to produce a full "monolayer" due to steric hindrance effects[14]; specifically the methyl groups may restrict access to surface bonding sites.

This study probes the growth of aluminium oxide on rutile TiO_2 by in-situ ALD using near-ambient pressure X-ray photoelectron spectroscopy (NAP-XPS). This technique allows us to monitor chemical information about the surface reactions as they happen at pressures in the mbar range. XPS is traditionally a high vacuum technique, but the ability to access pressures in the mbar range is making NAP-XPS a more relevant tool for in-situ studies of industrial processes. We have previously attempted similar experiments in ultra-high vacuum (dosing at $\sim 5 \times 10^{-8}$ mbar and purging to $\sim 1 \times 10^{-9}$ mbar) at room temperature where we found the growth was very inhomogeneous over the length scales accessible from the $\sim 100\,\mu$m measurement area. Further we found that the process did not behave as an "ideal" ALD reaction mechanism

[a] School of Physics, University of Nottingham, Nottingham, NG7 2RD, United Kingdom. E-mail: J.OShea@nottingham.ac.uk
‡ robert.temperton@nottingham.ac.uk

† Electronic Supplementary Information (ESI) available: [details of any supplementary information available should be included here]. See DOI: 10.1039/cXCP00000x/

* (cis-bis(isothiocyanato)bis(2,2'-bipyridyl-4,4'-dicarboxylato)-ruthenium(II)

View Article Online
DOI: 10.1039/C8CP06912C

in UHV as after complete cycles the water did not cause complete disassociation of the methyl groups from the absorbed TMA[15]. This implies it is critical to use higher pressures rather than maintaining an equivalent dose by exposing at low pressures for longer. On some surfaces it has been shown that the carbon from absorbed TMA is not removed at these lower pressures. For example the study by Detwiler et. al shows that although on Pd(111) the reaction works as expected at both 7×10^{-6} mbar and 0.1 mbar, on Pt(111) carbon species were not removed at 7×10^{-6} mbar but were removed at 0.1 mbar[16]. This group have also studied the process on the Cu(111) surface - the paper by Gharachorlou et al.[17] shows TMA does adsorb on the hydroxyl-free surface, but on the oxidised surface surface absoption is favourable and results in the reduction of copper atoms from Cu^{1+} to Cu^0.

The temperature of the sample is also highly significant. It has been shown by Levrau et al. that water is not reactive enough to dissociate CH_3 groups from TMA on a silica surface at 200 °C[18]. Measurements from Vandalon and Kessels are also consistent with this showing that temperatures greater than 200 °C are required for complete removal of CH_3 (also on SiO_2). From this observed temperature dependence they draw the important conclusion the water half cycle is a thermally activated reaction, unlike the TMA half cycle which they show is independent of temperature[19].

In this paper we discuss the surface chemistry observed at the titania/alumina interface by monitoring the reaction's half-cycles in-situ under conditions applicable to the real industrial ALD process.

2 Experimental methods

Experiments were performed on a SPECS Devi-sim NAP-XPS instrument comprising a UHV preparation/analysis chamber (5×10^{-10} mbar) and interchangeable near ambient pressure (NAP) cells that can be docked onto the front-end of a Phoibos 150 hemispherical analyser. This arrangement (often referred to as the Lund cell approach[20]) allows a sample to be prepared in UHV and be transferred to the near ambient pressure (NAP) cell without breaking vacuum. The aperture between the cell and analyser was a 300 micron nozzle. Monochromatic Al K-α X-rays ($h\nu \approx 1486.6$ eV), produced by an X-ray anode and ellipsoidal monochromator, entered the NAP-cell through a thin silicon nitride window which is transparent to the X-rays.

A TiO_2(110) rutile crystal was mounted and cleaned in the UHV chamber, by rounds of 1 kV argon ion sputtering and 800 K annealing, resulting in a clean surface with XPS measurements showing minimal contamination and Ti 2*p* spectra showing only a Ti^{4+} oxidation state (sputtering causes oxygen defects at the surface resulting in a large Ti^{3+} contribution[21]). The sample was then transferred into the NAP cell.

The cell used for this experiment allowed e-beam heating of the sample stage - for these measurements 450 K was used which was monitored by a calibrated thermocouple on the sample stage. This temperature was selected as it has been shown to produce the optimal growth rates[22]. The manipulator was counter-cooled using a constant flow of room temperature nitrogen gas in order to minimise thermal expansion of the manipulator stabilising the sample position. Two gas inlets to the cell were used. Tri-methyl aluminium (97%, Sigma Aldrich) and deionised water (from a Triple Red purification system further degassed by freeze pump thaw) were each connected to the cell by a UHV leak valve allowing alternate dosing of the vapours at the desired pressure of 1.0 mbar (monitored by a chemically resistant gauge). This pressure provided a good compromise between count rate (which decreases with increasing pressure) and operating in pressures relevant to "real" ALD processes. Between each half cycle, the cell was allowed to pump down, via the nozzle aperture, to below 1×10^{-2} mbar (the lowest pressure the gauge connected to the cell can measure) - this is analogous to the purge cycles used in conventional ALD to remove gas-phase precursor from the reaction cell.

XPS was measured with the analyser running in small area mode. Measurements in the UHV chamber were measured at a pass energy of 20 eV. In the cell, due to the reduced counts, a pass energy of 40 eV was used. The binding energy position of the Ti^{4+} $2p_{3/2}$ XPS peak was used for calibration. This was determined by calibration of the clean (UHV) data to the O 1s peak of the surface oxide to be 530.05 eV binding energy[23]. A Shirley background has been subtracted from the data in the line plots but not the 2D maps. Where the spectrum intensity is given as a "relative intensity", the intensities have been scaled according to the area under the Ti 2*p* region. Peak fitting has been done using a pseudo-Voigt function where the Lorentzian width has been fixed to 0.2 eV (to approximately match the core hole lifetime) and the Gaussian width was allowed to vary with the fit.

It is worth noting that continuous and extensive exposure of the sample (and gas molecules) to X-ray radiation is an inherent aspect of this genre of in-situ XPS study. The authors acknowledge that radiation damage of samples as a result of this exposure is commonplace, particularly for organic systems, but have seen no evidence of this during this experiment. This conclusion is drawn from comparison of subsequent measurements, where we see no change in spectral line-shapes, and from comparing the in-situ data with measurements taken post mortem on an area of the sample not exposed to the X-ray beam.

3 Results

O 1*s*, Ti 2*p*, C 1*s* and Al 2*p* XPS data showing the first half cycles of TMA (a-d) and water (e-h) are shown in Figure 1. In all the plots, grey dots show the spectra prior to exposure to the TMA/water vapour, purple dots during exposure and green dots after the cell has been evacuated.

We first consider the initial TMA half cycle (T1). Here spectra of the surface measured in the UHV chamber at room temperature (black line) prior to being transferred into the NAP-cell are included for reference where we see small amounts of aluminium and carbon consistent with residual TMA from the chamber absorbed on the surface. As one would expect when dosing TMA, we see an increase in both the carbon (Figure c) and aluminium (Figure d) species. In the case of Al 2*p*, we see a single peak at ~74.5 eV that remains the same shape when comparing during and after dosing. For the C 1*s* spectra measured during TMA dosing, we see two peaks at ~283.2 eV and ~284 eV. Once the cell is evacuated, the higher binding energy (~284 eV) peak vanishes.

View Article Online
DOI: 10.1039/C8CP06912C

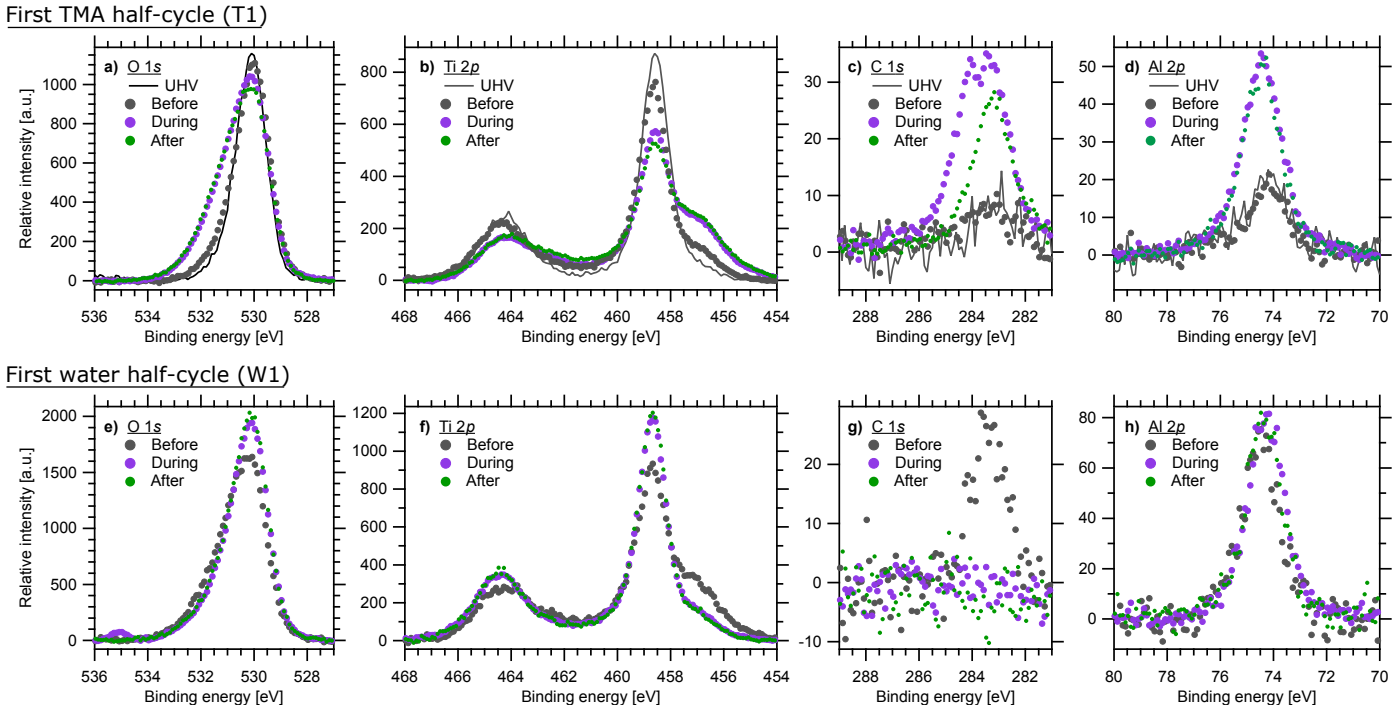

Fig. 1 In situ XPS measurements of the the first ALD cycle. For both the first TMA (a-d) and water (e-h) half cycles, O 1*s*, Ti 2*p*, C 1*s* and Al 2*p* regions are shown. For each, spectra measure before, during and after exposure to the precursor are shown. For the TMA half cycle, data measured in the UHV chamber (prior to being transferred to the NAP-cell) are included.

This peak is therefore assigned to the gas phase TMA molecules and the lower binding energy peak (∼283 eV) to TMA absorbed on the surface. We note that these binding energies are both surprisingly low (below even that of sp^2 hybridised amorphous carbon: 284.3 eV [24]). Other authors have however also observed the trimethylaluminium C 1*s* peak to be ∼283.4 eV [25] and the calibration method used here has been shown to be robust over numerous previous studies [26–29] repeatably placing aromatic carbon species at ∼285 eV on the TiO_2 (110) rutile surface.

In the O 1*s* (figure a) measured in UHV we see a single peak attributed to the TiO_2(110) surface oxide. In the cell, when TMA is dosed, we see a shoulder develop on the higher binding energy side. This is attributed to "non-lattice" oxygen species - most likely surface oxygen atoms reacting with absorbed TMA molecules. According to the half cycle reactions, the TMA reacts with OH groups, but this data suggests TMA can react directly with to the non-terminated bare rutile surface. The spectra remains a constant shape when the dosing is complete and the cell is evacuated.

The Ti data shows a doublet with the main $2p_{3/2}$ peak at ∼458.5 eV attributed to bulk Ti^{4+}. The lower binding energy shoulder at ∼457 eV represents Ti^{3+} species - this is identical to the established surface defects caused by Ar^+ ion sputtering. The Ti^{3+} feature is shown to increase in intensity during dosing. This is linked to the shoulder in the O 1s, when formation of OH or similar reaction with surface oxygen atoms causes some surface titanium atoms to be reduced into a lower oxidation state. After dosing has finished and the cell is evacuated, this Ti^{3+} feature remains.

On dosing the first water half-cycle, we see this Ti^{3+} shoulder reduce in intensity (Figure 1f) as the spectra returns to an almost defect free 4+ state. This is consistent with the concomitant O 1*s* (Figure 1e) where the relative amount of bulk oxygen increases. We also see a peak at ∼535 eV during water dosing which we assign to the gas phase. The carbon intensity (Figure 1g) is completely removed on dosing water and the aluminium peak remains the same intensity but shifts slightly to lower binding energy. We attribute this shift to the water stripping off the methyl groups leaving the aluminium bound with oxygen atoms. This behaviour is entirely consistent with the reaction cycles discussed in the introduction.

Subsequent cycles are shown in Figure 2. These maps show the same XPS regions as in Figure 1 but as a function of time, where progressing down the figure represents subsequent measurements. T2, T3 etc. and W2, W3 etc. indicate subsequent TMA and water doses respectively. The light grey lines show where the leak valve to the vapours were closed and the cell was allowed to pump down through the NAP-cone. The plots are split into two as measurements were paused here (overnight). Prior to cycle 5, we were measuring for much longer to properly characterise the binding energy shifts which are clearly shown in cycles 2 to 4.

These maps show very similar behaviour with subsequent cycles as the first two half cycles discussed above where all the spectral features discussed are repeatably visible. Here the Al 2*p* (Figures 2d and 2h) grows in intensity after each TMA cycle as one would expect. The shift to lower binding energy, happening after each water dose, is much clearer here. As with the first cycle, the water completely removed the methyl groups as

View Article Online
DOI: 10.1039/C8CP06912C

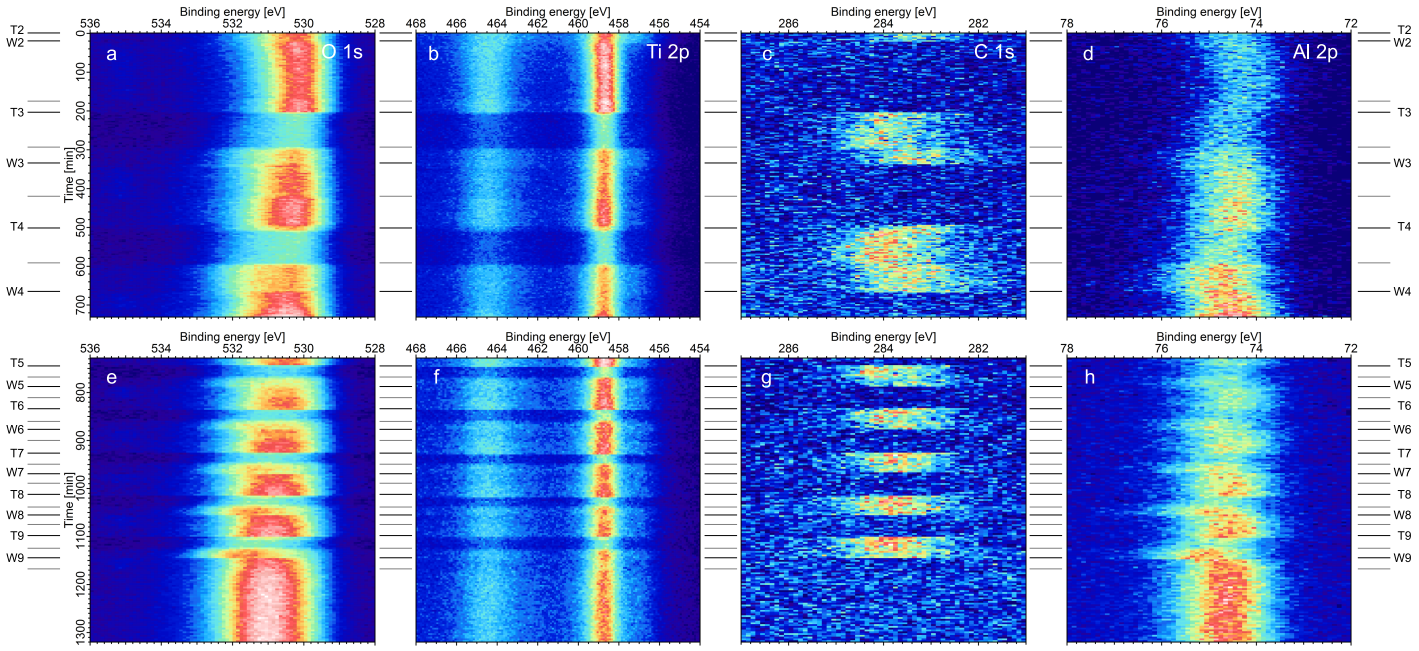

Fig. 2 In-situ XPS measurements during cycles 2-9, labaled T2-T9 and W2-W9 for TMA and water half-cycles respectivly. Grey lines indicate purges of the cell to 1e-2 mbar. From left to right, O 1s, Ti 2p, C 1s and Al 2p regions are showm. The break in the data (between plots a-d and e-h) represemts a break in the experiment, apart from which the measurements were continuous. Each cycle of the four regions took approximately 3 minutes 45 seconds to measure.

we see the carbon intensity (which is comparable for each TMA cycle) completely vanish after each water exposure. The O 1*s* shows a gradual change from predominately bulk TiO_2, to a mixture of titanium and aluminium oxides, to the aluminium oxide dominating by the final cycle. In the early cycles, we also see the same behaviour observed in the first cycle with the Ti^{3+} shoulder developing after TMA half-cycles and being reduced after dosing water.

It is worth noting that despite it appearing as if the intensities of features in the maps changing/moving within some cycles, this is attributed to small variations in the overall intensity - the peak shapes do not change. This is a result of small changes in the sample position due to thermal expansion of the sample stage (despite our best efforts to stabilise this by counter-cooling the manipulator and regular adjustment of the sample position to compensate).

4 Discussion

The fact that we see complete removal of CH_3 groups from absorbed TMA on exposure to water at 1 mbar and 450 K/177 °C is worthy of discussion. As mentioned previously Vandalona and Kessels investigation of the temperature dependence of this reaction shows 200 °C is not sufficient for complete removal of the the methyl groups (they see complete removal of CH_3 at 250 °C) [19]. Although we acknowledge that precise measurement of sample temperature in vacuum is a challenge, in this case our thermocouple was in contact with the sample and we do not observe uncertainties in our temperature measurement/control system of the order ∼50 K that would be implied here. We therefore do not think this discrepancy can be attributed to experimental uncertainty. The key difference between the Vandalona/Kessels study and this work is the duration of the exposure: Vandalona/Kessels investigate exposure times <0.2 s but here each cycle of the four XPS regions takes ∼4 min. Given that our time resolution is not comparable, we believe the datasets can not really be compared in this way and the two results are not necessarily as inconstant as they first appear - Vandalona/Kessels fit exponential functions to their time resolved coverage data and it is entirely possible that on the ∼0.1 s timescale we would still see ∼ 20% coverage they report for 200 °C [19].

The variation of the intensity of Ti^{3+} species is also very interesting as it is a non-constant throughout the experiment - it becomes less apparent for later cycles. This is explored in Figure 3 where spectra after each half-cycle (once the vapour has been pumped away) are presented, along with the line shape measured in the cell before exposure to either precursor as a reference. We see that after each TMA half cycle, the relative intensity of the Ti^{3+} feature becomes less intense until cycle 6 whereupon further cycles have no effect. This is likely due to steric hindrance effects: the size of the TMA molecule means that not all Ti sites are accessible to react with TMA until the water causes dissociation of the methyl groups. We therefore expect that the point we stop seeing the Ti^{3+} peak changing is the point we have aluminium oxide fully covering the titanium dioxide surface thus prohibiting further access to the TiO_2 by TMA molecules.

After water half-cycles, i.e. when each full cycle is complete, we see the Ti^{3+} defect heal to a progressively lesser extent after each cycle until cycle 6 where it stabilises. Our interpretation is that when the TMA is introduced, oxygen atoms on the surface break bonds with the Ti to form (O-Al) causing a change from Ti^{4+} to

View Article Online
DOI: 10.1039/C8CP06912C

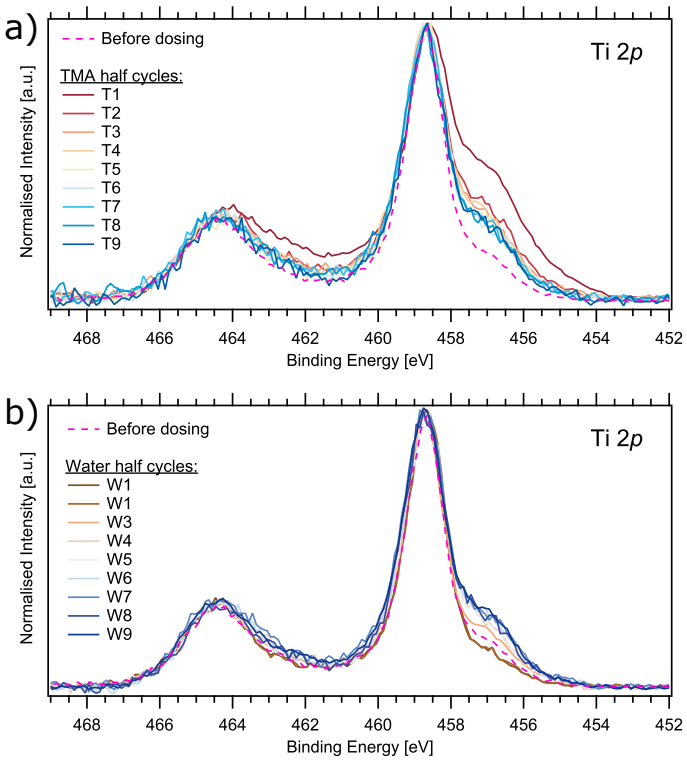

Fig. 3 Ti2p spectra after each TMA (a) and water (b) half cycles that have been normalised to the height of the $Ti^{4+}_{3/2}$ peak. A spectrum prior to dosing is included for reference.

Ti^{3+}. When water is dosed, these defects can be healed, causing a Ti-OH terminated surface at the vacancy sites. Depending on how the interface reconstructs after the formation of O-Al bonds, some defective Ti3+ atoms may be sub-surface. The implication of this is that there is not complete healing of Ti^{3+} to Ti^{4+} as a fraction of the defective Ti^{3+} is not accessible to water for hydroxylation. After each cycle, there are fewer and fewer Ti atoms available for bonding until cycle 6 where we reach complete alumina coverage of the surface. Subsequent cycles therefore have no effect on the underlying titania.

This mechanism doesn't preclude partial multilayer growth over regions covered by early cycles. Therefore by the point we have full coverage of the titanium dioxide surface, there may well be small regions of thicker coverage that are unreasonable with our $\sim$300 μm measurement area. Spectra were measured at multiple different positions on the sample (after the experiment) showing the final deposit was homogeneous on this macroscopic length-scale.

Figure 4 shows how ratios of the titanium/aluminium oxide O 1*s* peaks change in intensity after each full cycle, obtained by curve fitting the O 1*s* to two components at 530.0 eV and 530.9 eV to represent titania and alumina respectively. This exponential behaviour is consistent with the attenuation of electrons through a thin film as predicted by the Beer-Lambert law, implying relatively constant growth per cycle.

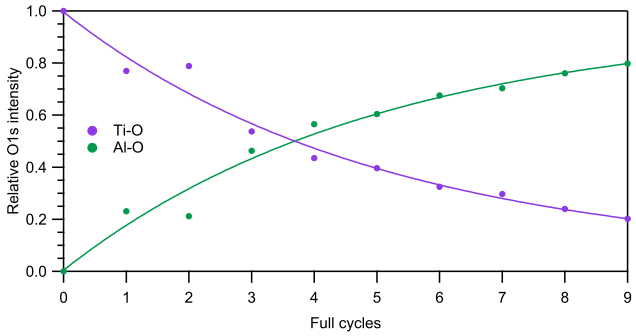

Fig. 4 Relative intensity of the O 1*s* signal attributed to the titanium and aluminium oxides (green and purple dots respectively) after each full cycle. Solid lines show exponential fits to the data.

5 Conclusions

We have used near-ambient pressure X-ray photoelectron spectroscopy (NAP-XPS) to monitor and characterise the atomic layer deposition of aluminium oxide on a titanium dioxide surface. We alternately exposed a clean rutile single crystal, held at 450 K, to1 mbar of trimethylaluminium and water until the point where the titanium dioxide was completely covered with aluminium oxide allowing us to probe the titania/alumina interface in-situ during these early cycles. We find an interesting oxidation state defect on the titanium dioxide surface that is formed on exposure to TMA and partially healed by exposure to water. The intensity of this Ti^{3+} defect relative to the Ti^{4+} peak in the Ti 2*p* XPS becomes stable after around 6 cycles where we believe we have reached full coverage of the surface. This defect then remains at this buried interface which has the potential to affect the electronic properties of the interface. Furthermore, at this pressure and temperature we find the reactions do behave like the model ALD process whereby the methyl groups are completely removed. We also find that the ALD process can be initialised on the bare surface oxide (without OH termination).

We would like to end by noting that this experiment entails a notable risk to the instrumentation used as the TMA-water reaction happens at room temperature. It is therefore very easy to coat various parts of the vacuum system that are sensitive to the deposition of films, such as gauges, with substantial quantities of aluminium oxide causing expensive damage. The authors therefore advise others to proceed with caution if they were to repeat this type of experiment.

6 Acknowledgements

The authors are grateful to the UK Energy Research Accelerator (Innovate UK) and the Engineering and Physical Sciences Research Council (EPSRC) for funding this work. Preliminary studies (detailed in Dr Andrew Gibson's PhD thesis[15]) were carried out on beamline I311 on the MaxII storage ring at MaxIV Laboratory (Sweden) and we are very greatful to Dr. Karsten Handrup and Dr. Karina Schulte for assistance with these experiments. Author are grateful to financial support for these early experiment from EPSRC, Molecularspray Ltd, and the European Community's Seventh Framework Programme (Grant No. FP7/2007-

View Article Online
DOI: 10.1039/C8CP06912C

2013) CALIPSO under Grant Agreement No. 312284.

References

1 B. O'Regan and M. Grätzel, *Nature*, 1991, **353**, 737–740.
2 C. Lin, F.-Y. Tsai, M.-H. Lee, C.-H. Lee, T.-C. Tien, L.-P. Wang and S.-Y. Tsai, *Journal of Materials Chemistry*, 2009, **19**, 2999.
3 T. W. Hamann, O. K. Farha and J. T. Hupp, *J. Phys. Chem. C*, 2008, **112**, 19756–19764.
4 C. Y. Neo and J. Ouyang, *Journal of Power Sources*, 2011, **196**, 10538–10542.
5 J.-Y. Kim, S. H. Kang, H. S. Kim and Y.-E. Sung, *Langmuir*, 2010, **26**, 2864–2870.
6 V. Ganapathy, B. Karunagaran and S. W. Rhee, *Journal of Power Sources*, 2010, **195**, 5138–5143.
7 S. Wu, H. Han, Q. Tai, J. Zhang, S. Xu, C. Zhou, Y. Yang, H. Hu, B. L. Chen and X. zhong Zhao, *Journal of Power Sources*, 2008, **182**, 119–123.
8 A. J. Gibson, R. H. Temperton, K. Handrup, M. Weston, L. C. Mayor and J. N. O'Shea, *The Journal of chemical physics*, 2014, **140**, 234708.
9 T. Suntola, *Materials Science Reports*, 1989, **4**, 261–312.
10 R. W. Johnson, A. Hultqvist and S. F. Bent, *Materials Today*, 2014, **17**, 236–246.
11 R. L. Puurunen, *Journal of Applied Physics*, 2005, **97**, 121301.
12 S. M. George, G. S. M., S. M. George and G. S. M, *Chem. Rev.*, 2010, **110**, 111.
13 A. C. Dillon, A. W. Ott, J. D. Way and S. M. George, *Surface Science*, 1995, **322**, 230–242.
14 R. L. Puurunen, *Chemical Vapor Deposition*, 2003, **9**, 249–257.
15 A. Gibson, *PhD thesis*, University of Nottingham, 2017.
16 M. D. Detwiler, A. Gharachorlou, L. Mayr, X.-K. Gu, B. Liu, J. Greeley, W. N. Delgass, F. H. Ribeiro and D. Y. Zemlyanov, *The Journal of Physical Chemistry C*, 2015, **119**, 150122160459000.
17 A. Gharachorlou, M. D. Detwiler, X.-K. Gu, L. Mayr, B. Klötzer, J. Greeley, R. G. Reifenberger, W. N. Delgass, F. H. Ribeiro and D. Y. Zemlyanov, *ACS Applied Materials & Interfaces*, 2015, **7**, 16428–16439.
18 E. Levrau, K. Van De Kerckhove, K. Devloo-Casier, S. Pulinthanathu Sree, J. A. Martens, C. Detavernier and J. Dendooven, *Journal of Physical Chemistry C*, 2014, **118**, 29854–29859.
19 V. Vandalon and W. M. M. Kessels, *Applied Physics Letters*, 2016, **108**, 1–6.
20 J. Knudsen, J. N. Andersen and J. Schnadt, *Surface Science*, 2016, **646**, 160–169.
21 M. J. Jackman, A. G. Thomas and C. Muryn, *Journal of Physical Chemistry C*, 2015, **119**, 13682–13690.
22 A. W. Ott, J. W. Klaus, J. M. Johnson and S. M. George, *Thin Solid Films*, 1997, **292**, 135–144.
23 J. Schnadt, J. N. O'Shea, L. Patthey, J. Schiessling, J. Krempaský, M. Shi, N. Mårtensson and P. a. Brühwiler, *Surface Science*, 2003, **544**, 74–86.
24 J. Díaz, G. Paolicelli, S. Ferrer and F. Comin, *Physical Review B*, 1996, **54**, 8064–8069.
25 S. Akhter, X. L. Zhou and J. M. White, *Applied Surface Science*, 1989, **37**, 201–216.
26 J. Taylor, L. Mayor, J. Swarbrick, J. N. O'Shea and J. Schnadt, *Journal of Physical Chemistry C*, 2007, **111**, 16646–16655.
27 L. C. Mayor, J. Ben Taylor, G. Magnano, A. Rienzo, C. J. Satterley, J. N. O'Shea and J. Schnadt, *The Journal of chemical physics*, 2008, **129**, 114701.
28 A. Rienzo, L. C. Mayor, G. Magnano, C. J. Satterley, E. Ataman, J. Schnadt, K. Schulte and J. N. O'Shea, *The Journal of Chemical Physics*, 2010, **132**, 084703.
29 M. Weston, T. J. Reade, K. Handrup, N. R. Champness and J. N. O'Shea, *The Journal of Physical Chemistry C*, 2012, **116**, 18184–18192.

View Article Online
DOI: 10.1039/C8CP06912C